J Intell Robot Syst (2014) 73:209–217
DOI 10.1007/s10846-013-9933-4

Control-Oriented Physical Input Modelling for a Helicopter UAV

Bryan Godbolt · Alan F. Lynch

Received: 11 July 2013 / Accepted: 12 September 2013 / Published online: 6 October 2013

Abstract It has become standard in the helicopter UAV control literature to use the main and tail rotor thrusts, and the main rotor flapping angles as inputs. However, the physically-controllable inputs are servomotors which actuate the main rotor cyclic and collective pitch, and the tail rotor collective pitch. Precise treatments of the helicopter model exist which study the physical inputs. However, these models remain intractable for practical implementation motivating researchers to use rough approximations such as simple gain relationships between thrust and collective. We propose and identify a physical input model which retains the accuracy of a general model but is algebraically simple enough for its use in control design. As a result of experimental validation, the vehicle's velocity is incorporated into the model to improve its accuracy.

Keywords Helicopter modeling and control · Helicopter thrust model · Model-based control · Helicopter UAV autopilot

B. Godbolt · A. F. Lynch (✉)
Applied Nonlinear Controls Laboratory, Department of Electrical and Computer Engineering, University of Alberta, Edmonton, Canada, T6G 2V4
e-mail: alan.lynch@ualberta.ca

B. Godbolt
e-mail: godbolt@ualberta.ca

1 Introduction

Small helicopters are uniquely suited to many applications such as monitoring crop conditions or inspecting infrastructure. Industrial-scale small helicopters provide increased payload and endurance as compared to other aircraft with similar flight capabilities (see [11] for a survey of rotorcraft). Therefore, helicopter research is relevant and includes topics such as navigation, control, and modelling.

A helicopter is actuated by four independent inputs: the main and tail rotor thrusts, and the main rotor flapping angles. These inputs are convenient for studying the helicopter control problem. However, these inputs cannot be directly controlled. Instead, servo motors are used to control the main and tail rotor collective pitch, and the main rotor cyclic pitch. Therefore, it might seem natural to design a control based on a model which includes the physical inputs. This type of modelling is well established in the literature [2, 4, 7, 15]. However, due to complexity it renders the control problem intractable. This complexity motivates experimental control work such as [14] where simple mappings are taken. Following work in [1, 2, 6, 14, 16, 18] we expect models which use thrust and flapping angles as inputs to be useful for control design. However, different than existing work we use experimental flight data to justify the reduction of models which are based

on physics to obtain invertible relationships for the physical inputs which are simple enough for implementation.

The organization of this paper is as follows. In Section 2 we present the dynamic model of the helicopter using the thrust and flapping inputs. The physical input models are derived in Section 3. Conclusions and future work are given in Section 4.

2 Modelling for Control Design

The helicopter model which is commonly used for control design is well established in the literature [6, 13, 17]. However, as mentioned above this model assumes direct control of the rotor thrusts and the main rotor flapping angles. Therefore, in order to use this model for control design it is necessary to map these control inputs to the physical inputs.

In addition to modelling the relationship between the control inputs and the physical servo inputs, there are many other effects which influence the helicopter dynamics. These effects include stabilizer fins, restorative moments due to the hingeless rotor, and stabilizing effects of the flybar. In particular, the flybar dynamics is a subject of wide interest since it is unique to small helicopters [3, 15]. However, this dynamics is inherently stable and therefore not required in the control design. Additionally, many small helicopters are now flybarless which implies these dynamics will become less relevant in the future. The general approach taken here is to ignore most of these effects and focus on aspects of the input models which can be shown to be practically significant.

In order to motivate the modelling work performed in the sequel, the generally-accepted model used for control design is presented here. For further details see [9]. The orientation of the helicopter is described using two coordinate frames: a navigation frame $\mathcal{N}$ with the orthonormal basis $\{e_1, e_2, e_3\}$, and a body-fixed frame with basis $\{e'_1, e'_2, e'_3\}$. The origin of $\mathcal{N}$ is fixed to the surface of the earth and its axes are oriented north, east, and down respectively. The body-fixed frame $\mathcal{B}$ has its origin fixed to the helicopter's center of mass and its axes oriented forward, right and down respectively. The helicopter dynamics are

$$\dot{p}^n = v^n \tag{1a}$$

$$m\dot{v}^n = mgR^T(\eta)e_3 + R(\eta)\begin{pmatrix} -T_M a \\ T_M b - T_T \\ -T_M \end{pmatrix} \tag{1b}$$

$$\dot{\eta} = W(\eta)\omega \tag{1c}$$

$$J\dot{\omega} = -\omega \times J\omega + \begin{pmatrix} z_M T_M b \\ z_M T_M a \\ x_T T_T - Q_M \end{pmatrix} \tag{1d}$$

where p^n and v^n are position and velocity in $\mathcal{N}$; m is mass; $\eta = (\phi, \theta, \psi)^T$ is the orientation expressed using roll-pitch-yaw Euler angles; $R \in SO(3)$ is the rotation matrix parametrized by η; W is the transformation between the body-fixed angular velocity ω and the derivatives of the Euler angles; J is the inertia matrix; T_M and T_T are the main and tail rotor thrusts; a and b are the longitudinal and lateral flapping angles; Q_M is the main rotor countertorque; and z_M and x_T are the main and tail rotor hub offsets in the e'_3 and e'_1 directions respectively. In order to obtain Eq. 1 we have neglected the tail rotor countertorque. Additionally, based on the helicopter's geometry we make the practical assumption $J = \mathrm{diag}(J_x, J_y, J_z)$ is diagonal. We remark that the coupling of the rotational inputs into the translational dynamics evident in Eq. 1b is a fundamental nonlinearity of the helicopter model. This effect renders the model non-minimum phase and therefore must be neglected to apply input-output linearization [13]. Indeed, a focus of our work elsewhere has been to incorporate these effects into the control design [8].

3 Physical Input Modelling and Identification

A straightforward approach to design a stabilizing control based on the above model assumes T_M, T_T, a, and b are inputs and Q_M is (at least approximately) known. In practice the helicopter is controlled using servomotor pulse widths as inputs. We denote the main and tail collective pitch servo pulse widths by δ_M and δ_T. The cyclic inputs are denoted δ_r and δ_p. The values of δ_r

and δ_p are normalized in order to remove the helicopter's calibration from the input mapping. Since the pilot often adjusts the cyclic trims as a result of changing environmental conditions or payload configuration, as a part of our regular preflight setup we read the calibration for the cyclic servos from the pilot's radio [10].

We must now establish relationships between the physical inputs δ_M, δ_T, δ_r, δ_p and the inputs used for control T_M, T_T, a, b. Our objective is to derive expressions of minimal complexity which retain sufficient accuracy to be practically useful. The experimental results presented in this section were collected using the Applied Nonlinear Control Laboratory (ANCL) helicopter UAV platform described in [9, 10].

3.1 Mapping from Main Rotor Thrust to Collective Pitch Servo

We begin our model simplification with the main rotor thrust. Expressions for this thrust are typically derived using first principles and in addition to collective pitch they depend on velocities as well as derivatives of flapping and coning angles [4, 15]. Many of these quantities are likely to be insignificant for the computation of thrust. For instance, the flapping angles are neglected in [7] for the thrust expression. For most practical trajectories, angular velocity only appears in transient and is therefore also unlikely to have a significant effect on thrust. As an initial approximation of the model we will assume a hover flight condition where all velocities are zero to simplify the general expression of the thrust model. We will show this model becomes inaccurate during vertical flight experiments. We rederive a simplified expression which includes vertical flight dependence and show it has improved accuracy.

A general model of thrust as given in [3, p. 162] is

$$T_M = \frac{\rho a_M c_M R_M N_b}{24}\Big\{\big(4(R_M\Omega_M)^2 + 6(u^2+v^2)\big)\Theta_M + 6R_M\Omega_M\,(w - v_i - va + ub) - 3R_M\Big(u(p+\dot{b}) + v(q+\dot{a})\Big)\Big\} \tag{2}$$

where Θ_M is the main rotor collective pitch; u, v, and w are the velocities in the e'_1, e'_2, and e'_3 directions respectively; p, q, and r are the components of the body-fixed angular velocity; Ω_M is the main rotor speed; ρ is the air density; R_M is the radius of the main rotor disk; N_b is the number of blades; a_M is the main rotor lift curve slope; c_M is the main rotor blade chord length; we have neglected the rotor coning angle; and v_i is the induced velocity

$$v_i = \frac{T_M}{2\rho\pi R_M^2\sqrt{(V\cos\alpha)^2 + (V\sin\alpha + v_i)^2}} \tag{3}$$

where V is the air flow speed and α is the angle of the airstream with respect to the rotor disk. Values for the parameters are given in Table 1. Based on the mechanical design of the helicopter we expect the main rotor thrust to depend on collective pitch and rotor speed. For example, by ignoring all of the terms in Eq. 2 except the one containing Θ_M and Ω_M we obtain the thrust model used in [14]. The caveat to this approach is it ignores the effect of the induced velocity. In [3] the alternative model

$$T_M = \Omega_M^2\Bigg(C_M\Theta_M + \frac{D_M^2}{4\pi\rho R_M^2} - \frac{D_M}{\sqrt{2\pi\rho}R_M}\sqrt{C_M\Theta_M + \frac{D_M^2}{8\rho\pi R_M^2}}\Bigg) \tag{4a}$$

$$C_M = \frac{\rho a_M c_M R_M^3 N_b}{6} \tag{4b}$$

$$D_M = \frac{2C_M}{3R_M} \tag{4c}$$

is derived which assumes no vehicle velocity. We attempted to validate this model by applying step inputs to the collective pitch using the pilot's radio. The results of this experiment are shown in Fig. 1 where the measured thrust is computed

Table 1 Main rotor parameters

R_M	0.89 m
N_b	2
a_M	6.6
c_M	0.066 m
C_D	0.005
α_M	−3490 μs/rad
β_M	1860 μs
k_p	0.10 rad
k_r	0.013 rad

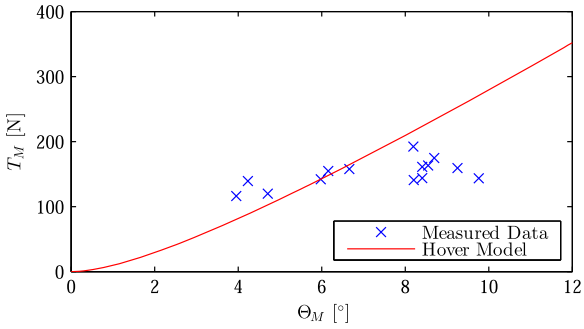

Fig. 1 Results of the hover model validation experiment. The *solid line* shows the thrust predicted by Eq. 4 and the measured values are denoted by ×

by differentiating the velocity. Except at hover (roughly 6° collective pitch), the model does not match the measured values. Figure 2 shows a typical response when a step input is applied. Rather than the constant acceleration we expected to measure based on Eq. 4, we observe that the vertical velocity quickly saturates. Therefore, we propose the inclusion of vertical velocity dependence in our thrust model. To proceed we simplify Eq. 2 by assuming $u = v = p = q = 0$ and obtain

$$T_M = C_M \Omega_M^2 \Theta_M + D_M \Omega_M (w - v_i). \tag{5}$$

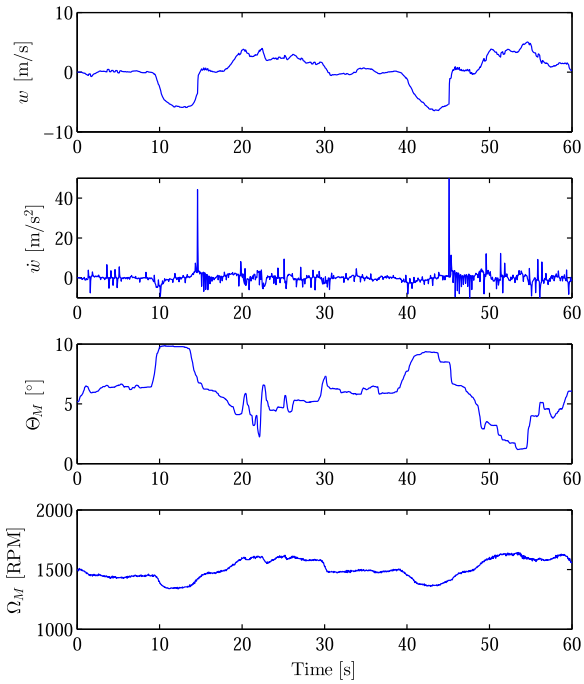

Fig. 2 Typical step response showing velocity saturation

Then taking either of the special cases $\alpha = \frac{\pi}{2}$ and $V = -w$ for climb, or $\alpha = -\frac{\pi}{2}$ and $V = w$ for descent we obtain the same simplification of Eq. 3

$$v_i^2 - w v_i - \frac{T_M}{2\rho\pi R_M^2} = 0$$

which can be solved to obtain

$$v_i = \frac{w}{2} \pm \sqrt{\frac{w^2}{4} + \frac{T_M}{2\rho\pi R_M^2}}. \tag{6}$$

Combining Eq. 6 with Eq. 5 and by enforcing $\Theta_M = 0$ when $T_M = 0$ we obtain

$$\Theta_M = \frac{1}{C_M \Omega_M^2}\left(T_M - \frac{D_M \Omega_M w}{2} + \frac{D_M \Omega_M}{\sqrt{2\rho\pi} R_M}\sqrt{T_M + \frac{\rho\pi w^2 R_M^2}{2}}\right) \operatorname{sgn} w.$$

However, for our current purpose we desire the inverse relationship which gives main rotor thrust in terms of collective

$$T_M = C_M \Omega_M^2 \Theta_M + \frac{D_M^2 \Omega_M^2}{4\rho\pi R_M^2} + \frac{D_M \Omega_M w}{2} - \frac{D_M \Omega_M}{\sqrt{2\rho\pi} R_M}\left(C_M \Omega_M^2 \Theta_M + \frac{D_M^2 \Omega_M^2}{8\rho\pi R_M^2} + \frac{D_M \Omega_M w}{2} + \frac{\rho\pi w^2 R_M^2}{2}\right)^{\frac{1}{2}}. \tag{7}$$

Remark that when $w = 0$ we obtain Eq. 4a.

Figure 3 shows the measured thrust as well as the output of models (4) and (7). The thrust model which includes vertical velocity (7) captures the saturation behaviour observed at times 38 s and 48 s evidenced by a transient net acceleration. However, the hover model (4a) predicts a steady-state net acceleration which is not supported by the data. Between 80 s and 90 s both models deviate from the measured values. This error is likely the result of a wind gust which caused additional lift. When a wind gust causes the helicopter to rise, the pilot reacts by decreasing collective to maintain altitude. Since neither model accounts for the wind, the measured decrease in collective causes both models to predict a decrease in thrust.

With our simplified relationship between thrust and collective complete, it remains to establish a mapping between the collective pitch and its

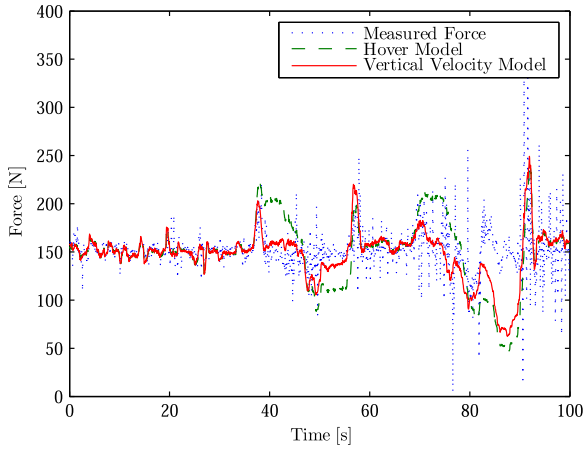

Fig. 3 Comparison of thrust models Eq. 7 (*solid line*) and Eq. 4a (*dashed line*), and the measured force (*dotted line*)

corresponding servo pulse width. This mapping will depend on the configuration of the helicopter as well as the particular servo used. The measurements for the ANCL Helicopter are shown in Fig. 4. The servo was found to exhibit a hysteresis resulting in different measurements if the pitch was sequentially increased or decreased. However, this difference is not expected to be significant in practice and so we fit the line

$$\delta_M = \alpha_M \Theta_M + \beta_M \tag{8}$$

to the entire data set. The parameter values are given in Table 1.

3.2 Mapping from Flapping Angles to Normalized Cyclic Inputs

Strictly speaking the flapping angles are controlled directly by the cyclic inputs but they are influenced by a stabilizing effect from the flybar [3, 4, 12, 15]. In addition, the hingeless rotor creates a restorative moment which influences the net torque on the aircraft [13, 17]. Since our goal is a simplified model which allows us to focus on the fundamental coupling present in the helicopter dynamics, we choose to ignore the additional dynamics. Indeed, the flybar dynamics are fast and stable. We therefore take a first-order, steady-state approximation of the mapping between the flapping angles and the cyclic inputs by using flight data where the pilot forced the rotational dynamics using a sinusoidal input to the cyclics. The data collected during this experiment is shown in Fig. 5. We expand the rotational dynamics in the roll and pitch directions as

$$J_x \dot{p} = qr(J_y - J_z) + z_M T_M b$$
$$J_y \dot{q} = pr(J_z - J_x) + z_M T_M a$$

and since $r = 0$ during this flight, we are able to isolate the flapping angles as

$$b = \frac{J_x \dot{p}}{z_M T_M}$$
$$a = \frac{J_y \dot{q}}{z_M T_M}$$

which results in the plots shown in Fig. 6. The parameter values are given in Table 2. We used

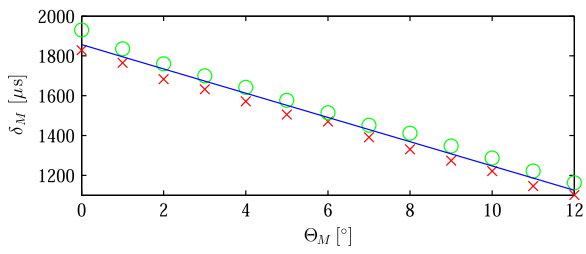

Fig. 4 Identified mapping from collective pitch to servo pulse width. The *circles* ∘ show measurements made while the pitch was being decreased, while the × show increasing pitch. The *solid line* shows the least squares fit

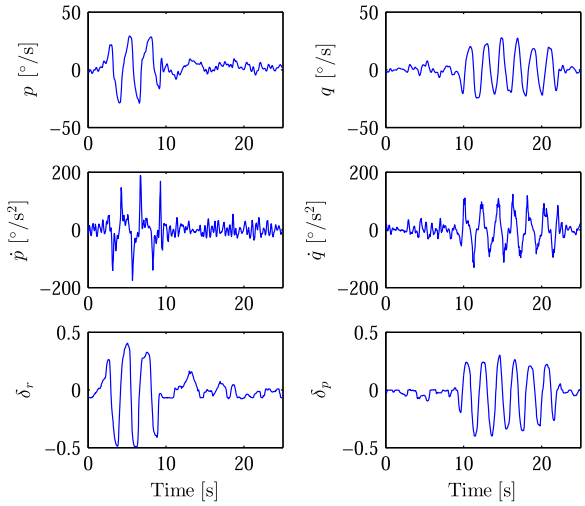

Fig. 5 *Cyclic input* identification data. The *pilot inputs* are normalized and therefore dimensionless

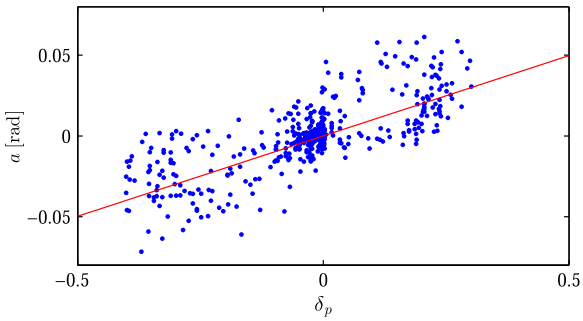

(a) Identification results for mapping from cyclic input to longitudinal flapping angle. The *solid line* shows $a = k_p \delta_p$

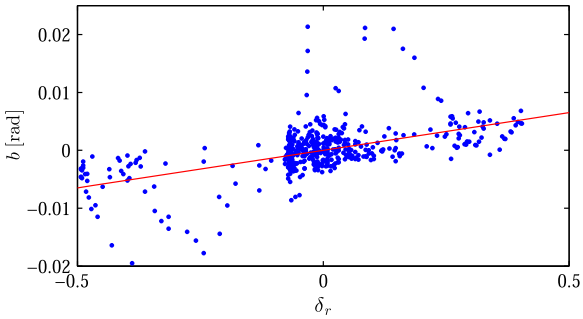

(b) Identification results for mapping from cyclic input to lateral flapping angle. The *solid line* shows $b = k_r \delta_r$

Fig. 6 Identification results for cyclic input to flapping angle mapping

a linear fit to approximate the mapping by the identified functions

$$a = k_p \delta_p \tag{9a}$$

$$b = k_r \delta_r \tag{9b}$$

where the values of the gains are given in Table 1. We remark that the gains differ by an order of magnitude.

Table 2 ANCL Helicopter parameters

J_x	0.36 kg m^2
J_y	1.48 kg m^2
J_z	1.21 kg m^2
m	15.5 kg
ρ	1.2 kg/m^3
z_M	0.32 m
x_T	1.06 m
g	9.81 m/s^2

Table 3 Tail rotor parameters

R_T	0.175 m
a_T	6.4
c_T	0.0325 m
α_T	−1590 μs/rad
β_T	1570 μs

3.3 Tail Rotor Thrust and Main Rotor Countertorque

The tail rotor thrust model is found using a hover assumption from [3]. However, different than [3] we include negative collective pitch. Ignoring negative collective is reasonable for the main rotor since it is not practically relevant for non-inverted flight. The negative collective pitch is included by defining T_T as

$$T_T = \Omega_T^2 \Bigg(C_T |\Theta_T| + \frac{D_T^2}{4\pi\rho R_T^2} - \frac{D_T}{\sqrt{2\pi\rho} R_T} \sqrt{C_T |\Theta_T| + \frac{D_T^2}{8\rho\pi R_T^2}} \Bigg) \operatorname{sgn} \Theta_T \tag{10a}$$

$$C_T = \frac{\rho a_T c_T R_T^3 N_b}{6} \tag{10b}$$

$$D_T = \frac{2C_T}{3R_T} \tag{10c}$$

where Ω_T is rotor speed, Θ_T is collective pitch, a_T is blade lift curve slope, c_T is blade chord length, and R_T is rotor disk radius. The parameter values are given in Table 3. Figure 7 shows T_T plotted over a practically relevant range of Θ_T. In the

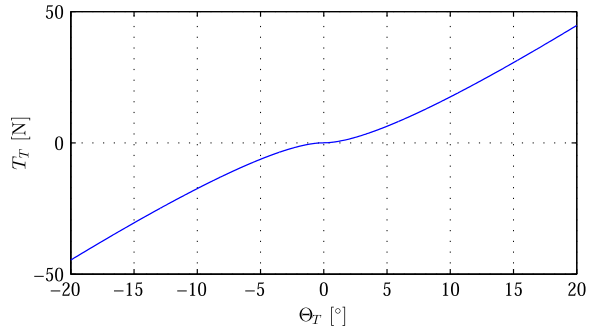

Fig. 7 Graph of T_T versus Θ_T

absence of rolling and pitching motion the yaw dynamics are

$$J_z \dot{r} = x_T T_T - Q_M \tag{11}$$

where the parameter values are given in Table 2. From Eq. 11 we remark that measuring $\dot{r}$ will not isolate the tail rotor thrust. Thus, we must consider the tail rotor thrust and the main rotor countertorque models simultaneously. We begin by using the countertorque model given in [3, Eq. 5.40]

$$Q_M = C_M^Q \frac{(T_M)^{(3/2)}}{\Omega_M} + D_M^Q \Omega_M^2 \tag{12a}$$

$$C_M^Q = \frac{1}{\sqrt{2\rho\pi} R_M} \tag{12b}$$

$$D_M^Q = \frac{\rho c_M R_M^4 C_D N_b}{8} \tag{12c}$$

where C_D is the drag coefficient. When Ω_M is assumed constant, Eq. 12 is the model used in [13].

As is widely discussed in the literature (see for instance [5]), it is common practice for a pilot to control the heading of a helicopter by providing a velocity reference to a gyro which controls the collective pitch of the tail rotor. If this gyro remains in the loop during autopilot control, its dynamics must be identified and typically inverted to perform collective control [5, 15, 18]. Here, we have chosen a configuration where the gyro is only used during manual flight. Thus, we only require a mapping from Θ_T to δ_T (which is analogous to Eq. 8 for the main rotor)

$$\delta_T = \alpha_T \Theta_T + \beta_T \tag{13}$$

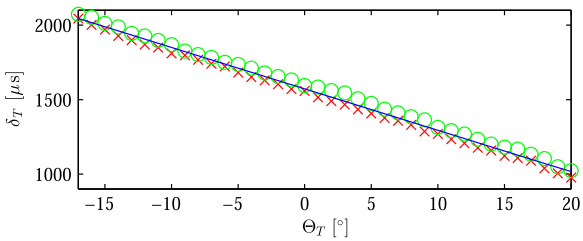

Fig. 8 Identified mapping between tail rotor collective pitch and servo pulse width. The *circles* ∘ show measurements made while the pitch was being decreased, while the × denote increasing pitch. The *solid line* shows the least squares fit

which is found by fitting data measured directly from the ANCL Helicopter and shown in Fig. 8. The parameter values are given in Table 3.

In Fig. 9 the thrust model (10) and countertorque model (12) are plotted using flight data where the pilot hovered the helicopter at a constant altitude in order to keep Q_M constant while varying T_T. The measured torque is computed by differentiating the heading. In order to calibrate Q_M for the period of constant heading, C_D was decreased from 0.016 as given in [3] to 0.005. At approximately 55 s there is a difference between the measured torque and the torque due to T_T. This abrupt increase in T_T is caused by an increase

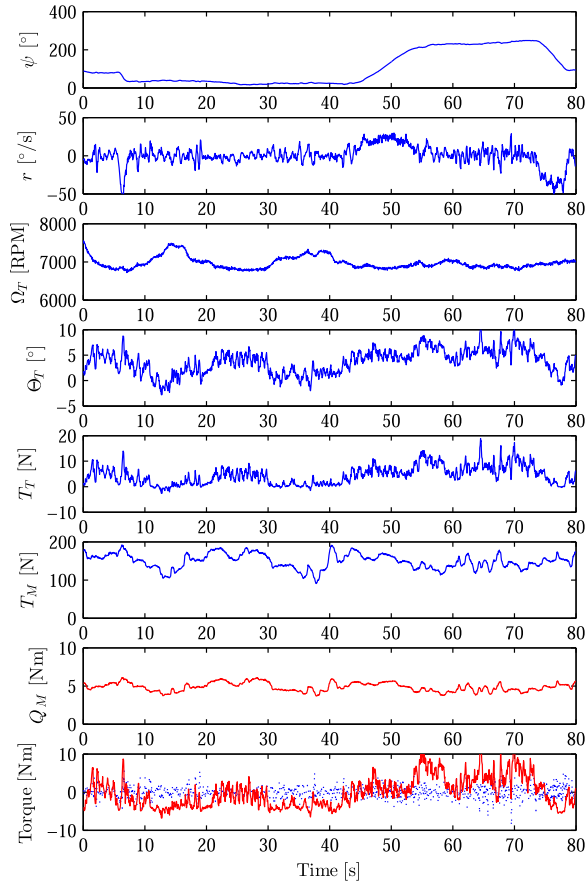

Fig. 9 Tail thrust model validation data showing a hover flight with fast large amplitude yaw motion. In the *bottom plot* the *dotted line* shows the measured net torque while the *solid line* shows the difference between the predicted torque due to the tail rotor and the main rotor countertorque

in Θ_T. Since we do not measure any resulting motion, this variation in tail thrust is likely due to a wind gust being rejected by the gyro. Without removing the gyro it is impossible to perform an experiment where T_T remains constant. However, we use a vertical climb flight which provides a variation in Q_M but no variation in heading. Since there is no variation in heading, we know the net torque should be zero. As shown in Fig. 10, the results using Eq. 12 provided a poor prediction of the countertorque during the climb.

As we did for T_M, we return to the general model of Q_M in [3] and preserve the vertical velocity terms while removing the effects of the lateral and angular velocities, as well as the flapping and coning angles. The resulting expression is

$$Q_M = -\frac{\rho a_M c_M R_M^2 N_b (w - v_i)^2}{4} - \frac{\rho a_M c_M R_M^3 N_b \Omega_M (w - v_i)}{6}\Theta_M + \frac{\rho c_M R_M^4 C_D N_b \Omega_M^2}{8}$$

which when combined with Eqs. 5 and 6 gives

$$Q_M = \left(-\frac{w}{2} + \sqrt{\frac{w^2}{4} + \frac{T_M}{2\rho\pi R_M^2}}\right)\frac{T_M}{\Omega_M} + D_M^Q \Omega_M^2. \tag{14}$$

Figure 10 shows that this model provides a much better fit for the climb data while reducing to Eq. 12 when $w = 0$ (as is the case for the flight shown in Fig. 9). Figure 11 shows how Q_M depends on T_M for a practically relevant set of constant w.

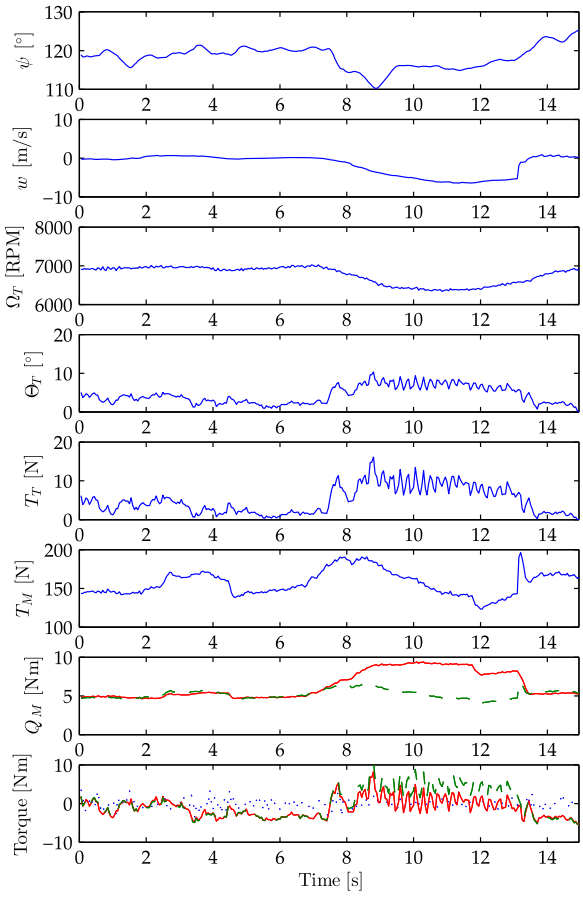

Fig. 10 Tail thrust and main rotor countertorque model validation data showing large variation in Q_M during fast vertical climb. In the *bottom two plots* the *solid line* uses the countertorque model with velocity dependence and the *dashed line* uses the hover model. In the *bottom plot* the *dotted line* shows the measured net torque

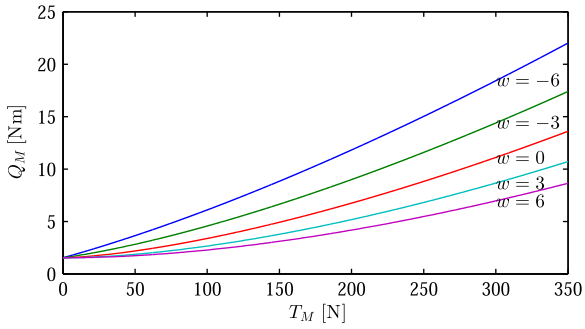

Fig. 11 Family of curves showing how Q_M depends on T_M for constant w. Units of w are m/s

4 Conclusions and Future Work

In order to apply a model-based control law it is beneficial to have a model which includes the physically-controllable inputs. However, precise treatments of this model are impractical for implementation of the control. Therefore, we propose a simplification of the thrust and countertorque models which is based on general modelling work in order to preserve structure derived from the physics. Different than previous work, we test the

modelling in experiment and identify large discrepancies during vertical flight which we address by rederiving the model including vertical velocity dependence. Despite the added complexity due to this added dependence, these expressions can be inverted explicitly. It is expected this work will prove useful for nonlinear model-based helicopter control. Future work includes investigating the practical effects of horizontal velocities on the thrust and countertorque models.

References

1. Abbeel, P., Coates, A., Quigley, M., Ng, A.Y.: An application of reinforcement learning to aerobatic helicopter flight. In: Proceedings of the Twentieth Conference on Advances in Neural Information Processing Systems. Vancouver, BC (2007)
2. Ahmed, B.: Autonomous landing of lightweight helicopters on moving platforms such as ships. Ph.D. thesis, The University of New South Wales at The Australian Defence Force Academy, Canberra, Australia (2009)
3. Barczyk, M.: Nonlinear state estimation and modeling of a helicopter UAV. Ph.D. thesis, Dept. of Electrical and Computer Engineering, University of Alberta, Edmonton, AB (2012)
4. Bisgaard, M.: Modeling, estimation, and control of helicopter slung load system. Ph.D. thesis, Aalborg University, Aalborg, Denmark (2007)
5. Cai, G., Chen, B.M., Lee, T.H.: Unmanned Rotorcraft Systems. Advances in Industrial Control. Springer-Verlag, London, UK (2011)
6. Castillo, P., Lozano, R., Dzul, A.E.: Modelling and Control of Mini-Flying Machines. Springer-Verlag, London, UK (2005)
7. Gavrilets, V., Frazzoli, E., Mettler, B., Piedmonte, M., Feron, E.: Aggressive maneuvering of small autonomous helicopters: a human-centered approach. Int. J. Robot. Res. **20**, 795–807 (2001)
8. Godbolt, B., Lynch, A.F.: A novel cascade controller for a helicopter UAV with small body force compensation. In: Proceedings of the American Control Conference, 2013, pp. 802–807. Washington, DC (2013)
9. Godbolt, B., Lynch, A.F.: Model-based helicopter UAV control: experimental results. J. Intell. Robot. Syst. (2014). doi:10.1007/s10846-013-9898-3
10. Godbolt, B., Vitzilaios, N.I., Lynch, A.F.: Experimental validation of a helicopter autopilot design using model-based PID control. J. Intell. Robot. Syst. **70**, 385–399 (2013)
11. Kendoul, F.: Survey of advances in guidance, navigation, and control of unmanned rotorcraft systems. J. Field Robot. **29**, 315–378 (2012)
12. Kim, S.K.: Modeling, identification, and trajectory planning for a model-scale helicopter. Ph.D. thesis, University of Michigan, Ann Arbour, MI (2001)
13. Koo, T.J., Sastry, S.: Output tracking control design of a helicopter model based on approximate linearization. In: Proceedings of the 37th IEEE Conference on Decision and Control, pp. 3635–3640. Tampa, FL (1998)
14. Marconi, L., Naldi, R.: Robust full degree-of-freedom tracking control of a helicopter. Automatica **43**, 1909–1920 (2007)
15. Mettler, B.: Identification Modeling and Characteristics of Miniature Rotorcraft. Kluwer Academic Publishers, Norwell, MA (2003)
16. Peng, K., Cai, G., Chen, B.M., Dong, M., Lum, K.Y., Lee, T.H.: Design and implementation of an autonomous flight control law for a UAV helicopter. Automatica **45**, 2333–2338 (2009)
17. Raptis, I.A., Valavanis, K.P., Moreno, W.A.: A novel nonlinear backstepping controller design for helicopters using the rotation matrix. IEEE Trans. Control Syst. Technol. **19**, 465–473 (2011)
18. Shim, H.: Hierarchical flight control system synthesis for rotorcraft-based unmanned aerial vehicles. Ph.D. thesis, Dept. of Mechanical Engineering, University Of California, Berkeley, CA (2000)